Environmental Science Advances

ROYAL SOCIETY OF CHEMISTRY

PAPER

View Article Online
View Journal | View Issue

Cite this: *Environ. Sci.: Adv.*, 2024, **3**, 1400

Fluorescent carbon dot embedded silica nanocomposites as tracers for hydrogeological investigations: a sustainable approach†

Venu Sreekala Smitha, * Parola Athulya, Kazhuthoottil Kochu Jayasooryan and Thoppil Ramakrishnan Resmi

The injected tracer technique using nanoparticles has evoked a lot of research interest in hydrogeological research as it encompasses a broad spectrum of applications in water resource management. The present work deals with developing carbon dot embedded silica-based nanocomposites using a microwave-assisted co-polycondensation method. The synthesized carbon dot-embedded silica nanocomposites have been characterized for their structural and functional characteristics using UV-visible spectroscopy, photoluminescence spectroscopy (PL), lifetime analysis, Raman spectroscopy, Scanning Electron Microscopy (SEM), Transmission Electron Microscopy (TEM), Fourier Transform Infrared spectroscopy (FTIR) and X-ray Diffractometry (XRD). The results obtained showed that carbon dots having a size of less than 5 nm had been successfully embedded into the silica structure, and the nanocomposite as such shows interesting optical properties. Laboratory scale column experimental studies were further conducted to ascertain the applications of the synthesized carbon dot-embedded silica nanocomposite for hydrological studies. Experiments were performed by varying the filling materials (sand/soil) in the column during which different concentrations of the nanotracer were injected under the continuous flow of water at a constant flow rate of 5 ml min^{-1} followed by monitoring the detection of carbon dots for a definite time. The developed nanocomposite was found to exhibit satisfactory results in terms of the detection and recovery of carbon dots when injected as a tracer in an experimental hydrological study. About 99% of the nano tracer could be regained when ~0.5 g of the CD-SiO_2 nanotracer is injected into the column and the detection was much faster with a peak detection time of 6 minutes. The better traceability and retention of the original optical properties of the developed tracer under different experimental conditions could be attributed to the optimal size of the nanocomposite system. Thus, the current challenges faced in groundwater flow analysis such as huge time consumption/expenses can be resolved to a significant extent considering the better traceability of the developed nanotracer.

Received 14th May 2024
Accepted 27th July 2024

DOI: 10.1039/d4va00156g

rsc.li/esadvances

Environmental significance

The present manuscript is on the development of a functional nanocomposite material based on carbon dots and silica to enable its use as a nanotracer suitable for groundwater studies. The source, mixing dynamics, and flow of water resources can be easily understood when such environmental tracers are used as a tool and various information related to the flow direction, flow velocity/residence time, extent of mixing, and the properties of the flow matrix could be easily derived which may help significantly in the water management at specific sites. Thus, the nanocomposite tracer developed may help significantly in the sustainable management of water resources.

Introduction

The global demand for fresh water is expected to increase significantly (33%) by 2050 due to the rapid growth in population and the escalated activities in the agricultural and industrial sectors.[1] Pollutants that are discharged owing to the various anthropogenic activities are setting enormous pressure on the water bodies creating adverse effects on the sustainability of the environment.[2] A proper analysis of the

Ecology and Environment Research Group, Centre for Water Resources Development and Management (CWRDM), Kunnamangalam P. O., Calicut-673571, Kerala, India. E-mail: smithavs@cwrdm.org

† Electronic supplementary information (ESI) available: Photographs of the carbon dots synthesized from glucose and ethylene diamine at different microwave irradiation timings, results of the lifetime of the as-synthesized carbon dots, photographs of the synthesized carbon dot-embedded silica nanocomposites, and their PL decay curves. See DOI: https://doi.org/10.1039/d4va00156g

characteristics of various hydrological processes is hence required to detect the original source of pollution and to determine the transport behavior of various pollutants. Tracer technology has been demonstrated as a viable and efficient method for the characterization of various hydrological processes as it has the advantage of investigation from the laboratory scale to the field scale.[3] Hence it has become extremely important to develop tracers suitable for hydrological investigations from which unique information regarding various physicochemical and biological properties of the system can be gained.[4]

Tracers are generally used to track the movement of water through an aquifer system with which different types of water can be distinguished and the hydraulic and bio-geochemical processes involved can be determined.[5,6] Environmental tracers have a specific imprint on a particular system and hence play an important role in the detection and analysis of various pollutants.[7] Environmental tracers are used in many countries nowadays for the effective management of available water resources.[8] Thus, the source, mixing dynamics, and flow of water resources can be easily understood when environmental tracers are used as a tool.[9]

Tracers can be natural, artificial, or anthropogenic. Natural tracers are the ones that are pre-existing in the system while artificial tracers are intentionally added to a particular system for certain investigations.[10] Anthropogenic tracers usually occur as a by-product of certain processes or accidental additions. An ideal tracer should be environment friendly, non-toxic, chemically stable, able to get transported along with water, and should not get adsorbed, exchanged, or filtered along the flow path.[4] Moreover, it should not be present already at high concentrations, should not transform quickly, and must be detectable even at low concentrations.

Currently, different types of tracers are being used for characterizing aquatic flow systems such as salt tracers, dye tracers, isotope tracers, *etc.*[11] Conventional chemical tracers and radioactive tracers are known to be environmentally hazardous[12] which limits their use whereas non-radioactive tracers pose limitations due to their dimension. Non-radioactive tracers have high values for diffusion coefficient and as a result, when injected into a water resource, they may diffuse into rock strata resulting in a longer time to come out.[13] Moreover, a large amount of molecular tracer needs to be injected considering the low recovery rate and minimum threshold concentration for their detection.[14]

Colloidal nanoparticles with unique physical and chemical properties that are easily dispersed in water can have high transportability and low retention in porous media and hence qualify for injected tracer application.[15] The main advantage of a nanoparticle tracer is its modular structure and tunable properties. On the other hand, nanoparticles exhibit lower values of diffusion coefficient than molecular tracers because of their colloidal dimensions that reduce the extent of diffusion[1] which reduces the travel time between the resources when used as tracers.[16] Berson *et al.* in 2024 have introduced a novel approach to reporting nanoparticle tracers (RNTs) in which RNTs are employed in flow-through experiments emulating flow in a porous aquifer.[14] Two-layer architecture of nanoparticles encompassing an inner enclosed core and a porous outer shell, both doped with different fluorescent dyes for dual emission, has been attempted which offers a modular system with improved characterization and monitoring capabilities.

Nanoparticle tracers derived from cheap precursors such as carbohydrates,[17] agricultural materials,[18] and renewable organic materials[19] are more eco-friendly and can provide sustainable solutions for hydrological investigations when used as tracers. Carbon dots, an emerging class of carbon-based nanomaterials with a size of less than 10 nm have excellent water solubility and tuneable physicochemical and fluorescence properties, low toxicity, and good chemical stability, and are hence an ideal tracer material for characterizing aquatic flow systems.[20]

Large-scale synthesis and testing of carbon quantum dots (CQDs) towards their application as hydrogeological tracers were conducted by Warsi *et al.* in 2020 in which surface passivation of the carbon dots using polystyrene sulphonate was done to preserve their optical properties.[21] Carbon quantum dots have been used as a tracer for water seepage sources and pathways in grottoes recently by Sun *et al.* in which they have observed the strong transportation ability of carbon dots in water flow but with a limitation of fluorescence decay of the carbon dots after flowing through the rock sample.[22]

Even though carbon dots are used for tracer-related studies, a nanocomposite of carbon dots with silica as a tracer has not been reported yet. The advantage of a nanocomposite tracer comprising carbon dots and silica is that the carbon dots can be immobilized over the spherical silica particles *via* electrostatic interactions which addresses the issue of aggregation of nanoparticles and may help in improving the emission characteristics to a considerable extent.

The present work is an attempt towards the development of a carbon dot embedded silica-based nanocomposite, a functional nanocomposite material and to enable its use as a nanotracer suitable for groundwater studies. Laboratory-scale continuous flow column experiments were conducted further using the synthesized nanotracers to determine the practical applicability of the developed material for effectively managing the water resources.

Results and discussion

Characterization of the carbon dots

The photoluminescence (PL) behavior of carbon dots is considered the most fascinating property from a fundamental and applied perspective.[23] Carbon dots synthesized in the present work exhibit different colors in solution under daylight and UV light as shown in Fig. 1a and b. PL emission spectra of the as-synthesized carbon dots were recorded at an excitation wavelength of 320 nm and the results are provided in Fig. 1c. PL spectra of the carbon dots consist of dual-wavelength blue-green emissions with PL peaks positioned at the wavelength ranges of about 470 to 490 nm and 490 to 560 nm, respectively. The photoluminescence behavior of carbon dots is attributed to the charge or energy transfer processes associated with the electron-donating or accepting nature of carbon dots when

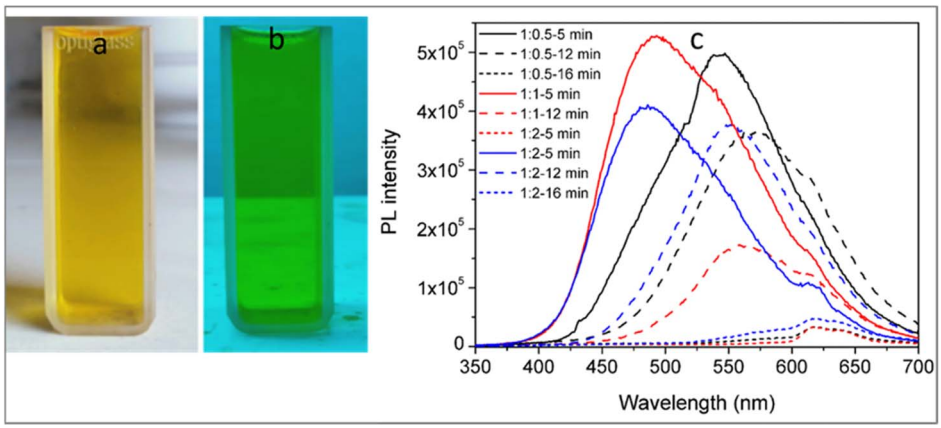

Fig. 1 (a) Photograph of the as-synthesized carbon dots under daylight, (b) intense green emission of the carbon dots under UV light and (c) photoluminescence spectra of the carbon dots prepared from glucose : ethylene diamine (G : ED) weight ratios from 1 : 0.5, 1 : 1 and 1 : 2 and microwave treated for 5, 12 and 16 minutes.

excited with light of a suitable wavelength.[24] The existence of different emissive surface states on the surface of the carbon dots arising out of the hybridization of the carbon skeleton and connected chemical groups is also considered the dominant luminescence origin.[25]

The photoluminescence emission intensity and wavelength were found to be dependent on the synthesis conditions followed. Microwave treatment of the precursor solution containing varying concentrations of glucose and ethylene diamine was carried out at 5 min, 12 min, and 16 min in the present work and it was found that the emission intensity decreased with microwave irradiation time whereas the fluorescence emission changed from green to red with increased microwave irradiation time. This correlation of photoluminescence with microwave irradiation time can be attributed to the particle size changes occurring to the carbon dots as a result of microwave irradiation.[26] The variation in the microwave irradiation time from 5 to 16 min causes variation in the sizes of the carbon dots synthesized which is responsible for the difference in the position of the emission peak. As the size of the carbon dots decreases, the energy gap will increase and *vice versa* due to the quantum confinement effect.[27]

Larger carbon dots will be excited at relatively longer wavelengths and the smaller ones will be excited at lower wavelengths and the intensity of PL relies on the number of particles excited at a particular wavelength. Moreover, an optimal microwave irradiation time is reported to increase the formation of functional groups mediated emission traps or hybridization changes to the carbon cores and π domains on carbon dots. An increase in the microwave irradiation time may destroy the surface structure of carbon dots which is attributed to the decrease in the fluorescence intensity.[28] The highest PL intensity was observed for the carbon dots prepared from G : ED ratio 1 : 1 and microwave treated for 5 minutes which could be due to the synergistic effect arising from the surface and core conditions of the carbon dots. The PL intensity decreases with microwave irradiation time, as it is dependent on the concentration of the carbon dots formed. An increase in the concentration of the carbon dots formed at long microwave irradiation times of 12 and 16 minutes may result in an increased interaction among the different polar groups causing reduced emission intensity. The high concentration of polar functionalities at high carbon dot concentration is known to cause agglomeration.[29]

Thus, the interesting photoluminescence behavior of the synthesized carbon dots such as a shift in the emission peak wavelength and its intensity is due to the particle size variation with microwave irradiation time and the difference in the distribution of the surface energy traps of the carbon dots. The color of the carbon dots also changes from yellow to orange and brown as the microwave irradiation time increases from 5 min to 12 min and 16 min, as shown in Fig. S1.† Fig. 2 represents the time-resolved PL decay curve for the carbon dots which shows that the data can be fitted to tri-exponential curves. The average lifetime and the three different components τ_1, τ_2, and τ_3 of the carbon dots synthesized under different conditions are tabulated (Table S1†). PL decay lifetime is an intrinsic property of carbon dots that refers to the time spent in the excited state

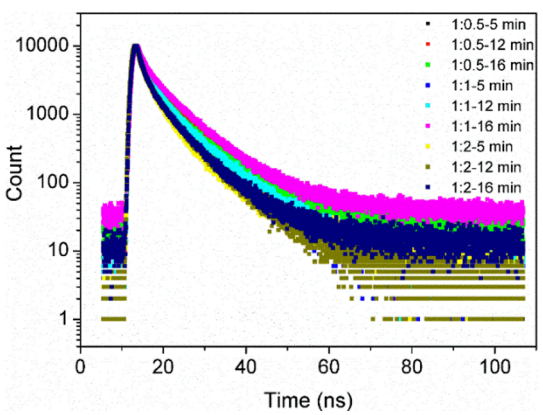

Fig. 2 PL decay curve of carbon dots prepared from glucose : ethylene diamine (G : ED) weight ratios from 1 : 0.5, 1 : 1 and 1 : 2 and microwave treated for 5, 12 and 16 minutes.

before returning to the ground state with the emission of photons. However, the duration of the lifetime can provide information regarding the PL mechanism of the carbon dots.[30] The obtained lifetime results of the carbon dots from the three components shed light on the recombination processes in the carbon core and the surface states.[31] It was observed that a short decay lifetime was dominant at shorter excitation wavelengths which is attributed to the relaxation of carriers from the carbogenic core to the surface of carbon dots.[32]

The absolute photoluminescence quantum yield (PLQY, ϕ_F) is an essential photophysical characteristic of carbon dots and the PLQY of the synthesized carbon dots (G : ED ratio 1 : 1, MW-5 min) was measured in percentage using a fluorescence spectrophotometer equipped with an integrating sphere detector. Under 344 nm excitation, the carbon dots emitted blue light with a quantum yield of 5.18 ± 0.001%.

A zeta potential value of −18.7 mV as measured using a Zetasizer (Anton Paar Litesizer 500) indicates that the carbon dots have a negative surface charge thus revealing the presence of negatively charged carboxyl (–COOH) and hydroxyl (–OH) functional groups on their surface. A reasonably good colloidal stability of the carbon dots[33] was revealed by the zeta potential measurement (Fig. S2†). Fig. 3 represents the transmission electron microscopic (TEM) images of the carbon dots synthesized from varying ratios of glucose and ethylene diamine and microwave-treated for about 16 minutes. The dark spots indicated the formation of nearly spherical clusters of carbon atoms that show a slight aggregation behavior with respect to the increase in ethylene diamine ratio. It was observed that the particle size of the carbon dots varied from ~10 nm to ~13 nm and to ~20 nm when the ratio between glucose and ethylene diamine was increased from 1 : 0.5 to 1 : 1 and 1 : 2. The high-resolution images obtained show the lattice fringes corresponding to the (002) and (100) plane of graphitic carbon.[34]

The selected area electron diffraction images obtained for the samples are provided as the inset which consists of a diffused halo without any spots or rings revealing the predominant amorphous behavior of the samples synthesized. Uniform-sized carbon dots were obtained when the ratio between glucose and ethylene diamine was 1 : 1. Carbon dots prepared from glucose and ethylene diamine in the ratio of 1 : 1 and microwave treated for 5 min were subjected to further characterization, considering the higher PL intensity obtained.

The UV-visible absorbance characteristics of the carbon dots were elucidated from the UV-visible spectra in which strong absorbance at around 327 nm and a relatively small peak at 235 nm were observed (Fig. 4a). The peak around 235 nm can be assigned to the π–π* transitions of sp^2 carbon (C=C bonds) indicating the presence of a graphitic carbon core.[35] The absorbance at 327 nm is attributed to the n–π* transition of C=O bonds in carbon dots.[36] Fourier Transform Infrared (FTIR) spectra of the carbon dots were recorded further and are presented in Fig. 4b. A very broad band around 3300 cm^{-1} corresponds to O–H/N–H stretching vibrations of the hydroxyl

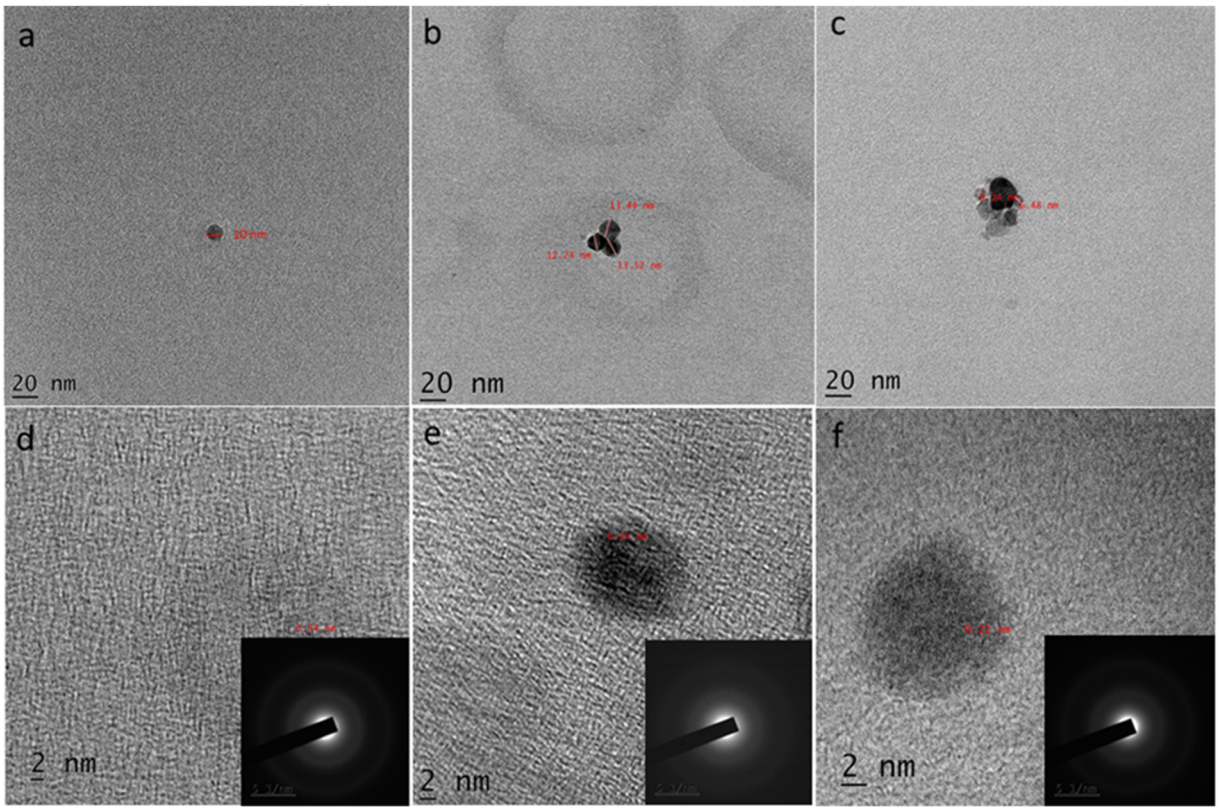

Fig. 3 Transmission electron microscopic (TEM) images of carbon dots prepared from glucose and ethylene diamine in the ratio (a and d) 1 : 0.5, (b and e) 1 : 1 and (c and f) 1 : 2, microwave treated for about 16 minutes (SAED pattern of the samples are shown in the inset).

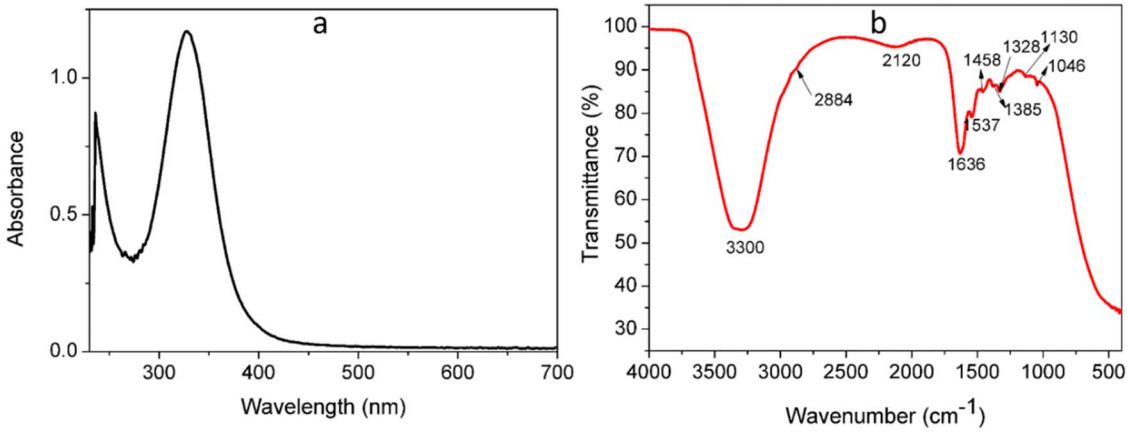

Fig. 4 (a) UV-visible absorbance spectra of carbon dots synthesized from glucose and ethylene diamine in the weight ratio 1 : 1 and microwave-treated for 5 minutes and (b) FTIR spectra of carbon dots synthesized from glucose and ethylene diamine in the weight ratio 1 : 1 and microwave treated for 5 minutes.

groups.[37] The small peak at 2884 cm^{-1} could be ascribed to C–H methyl group asymmetrical stretching. The small broad peak around 2120 cm^{-1} corresponds to the C–O stretching vibration. The characteristic peak at 1636 cm^{-1} corresponds to that of the graphite core of C=C stretching vibrations in C-dots.[38] The stretching bands of C–O (alkoxy) are observed at 1046 cm^{-1}. The signals at 1087 cm^{-1} obtained for the carbon dots correspond to the C–O stretching vibration. The small peak around 1537 cm^{-1} is assigned to the bending mode of N–H vibration whereas the one at 1458 cm^{-1} corresponds to the CH_2 group. The peak at 1328 cm^{-1} was assigned to the elongation vibration of the –COO bond indicating carboxyl groups, and the one at 1385 cm^{-1} indicates the presence of amide C–N bonds. The small peak at 1134 cm^{-1} is assigned to the carbonyl stretching vibration.

The presence of various functional groups such as hydroxyl, carbonyl, and carboxyl was detected in the carbon dots synthesized which may create emissive traps between π and π^* of C–C. Thus, the photoluminescence effect shown in the carbon dots is speculated to be due to the surface defects and size effects.[39]

Characterization of the carbon dot embedded silica nanocomposite

Carbon dot embedded silica nanocomposites (CD-SiO_2) were synthesized further by following a microwave-assisted co-polycondensation method as shown in Fig. S3.† The UV-visible absorbance characteristics of the carbon dot embedded silica (CD-SiO_2) nanocomposite were elucidated further (Fig. 5).

Pure carbon dots exhibit strong absorbance at around 320 nm which is attributed to the n–π^* transition of C=O bonds in carbon dots. For the carbon dot embedded silica nanocomposite, a peak at 275 nm corresponding to the π–π^* transition of the sp^2 carbon (C=C bond) indicating the presence of the graphitic carbon core and a shoulder peak at around 320 nm were also observed. The absorbance of carbon dots was within the UV region extending up to ~360 nm whereas for the CD-SiO_2 nanocomposites, the absorption tail extended up to about 500 nm. This increased absorbance in the visible region could be ascribed to the interaction between carbon dots and silica particles.

PL emission spectra of the carbon dot embedded silica nanocomposites were recorded at an excitation wavelength of 320 nm and the results are provided in Fig. 6a. Pure carbon dots are found to be strongly emissive upon excitation at wavelengths covering the ultraviolet to the visible region with an emission maximum of around 490 nm. The intensity of PL emission was found to decrease with an increase in the concentration of silica in the case of CD-SiO_2 nanocomposites. The PL of carbon dots is known to be affected by the concentration changes and there exists a critical concentration at which the distance between the luminescence centers is optimum (critical distance) causing maximum PL intensity. It is reported that, at low concentrations of C-dots, the distance between the luminescence centers is greater than the critical distance and may lead to a redshifted PL peak and quenching.[27]

The concentration of C-dots is relatively higher in the nanocomposite (CD-SiO_2-1:0.05), and hence the PL peak shows a blue shift (~455 nm) when compared to other samples

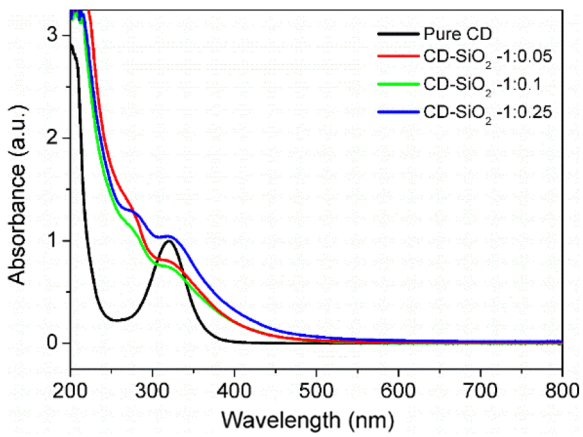

Fig. 5 UV-visible absorbance spectra of pure carbon dots and carbon dot embedded silica nanocomposites.

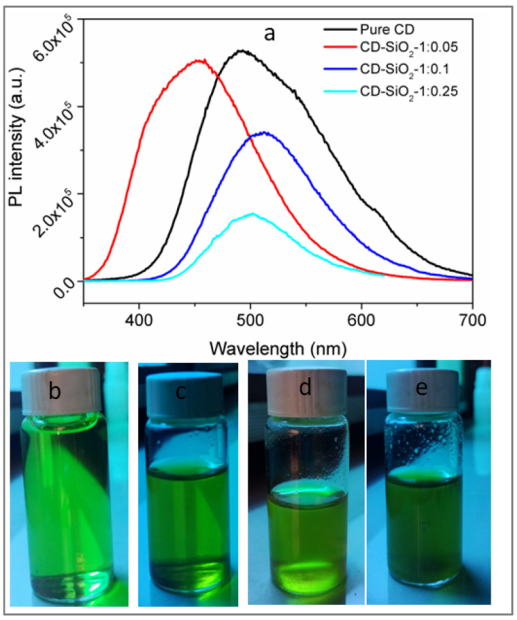

Fig. 6 (a) Photoluminescence spectra of carbon dots and carbon dot embedded silica nanocomposites recorded at an excitation wavelength of 320 nm and (b–e) photographs showing the emission behaviour of carbon dots and carbon dot embedded silica nanocomposites under UV light.

containing a lower concentration of C-dots (CD-SiO_2 1:0.1 and CD-SiO_2 1:0.25) which is characterized by a redshifted PL (peaks located at ~510 and 500 nm respectively) along with a quenching behavior. The results obtained for the PL of CD-SiO_2 nanocomposites in the present work are consistent with the reported results by Chen *et al.*, in 2014, in which they measured the PL response of the silica–carbon dot hybrids containing different concentrations of silica.[40]

The time-resolved PL decay curve of the C-dots and C-dot embedded silica nanocomposites was also recorded (Fig. S4†) which shows that the data can be fitted to tri-exponential curves. The average lifetime and the three different components τ_1, τ_2, and τ_3 of the samples synthesized are tabulated (Table 1). The average lifetime of the CD-SiO_2 nanocomposites was higher than that of pure carbon dots. This slower decay time of the carbon dots embedded in silica indicates the interaction between C-dots and silica causing alterations in their extent of bonding.[29]

The X-ray diffractogram and Raman spectra of the carbon dot embedded silica nanocomposite are shown in Fig. 7. Raman spectra depict a band at around 810 cm^{-1} which can be attributed to the symmetric Si–O–Si stretching in the nanocomposites.[41] Bands that spread from 910 cm^{-1} to 1030 cm^{-1} are assigned to multi-phonon scattering from silicon. The bands placed around 1090 cm^{-1} and 1200 cm^{-1} are assigned to Si–O stretching vibration. The presence of embedded carbon dots in the nanocomposite samples was apparent in the two major broad peaks at around 1329 cm^{-1} and 1587 cm^{-1} close to the D (disorder) and G (graphite) bands.[42]

The D band typically arises from the disordered graphite structures in the C-dots whereas the G band is related to crystalline graphite (E_{2g} mode) and the vibration of sp^2-bonded carbon atoms. The band at 1450 cm^{-1} could be assigned to the CH_2 scissor mode in the core of CDs.[43] OH bending features could also be observed around 1640 cm^{-1}. Thus, both amorphous and crystalline carbon phases are present in the core of the embedded CDs in silica as previously reported.[26]

The morphology of the CD-SiO_2 nanocomposites is presented in the SEM images below (Fig. 8).

The size distribution of silica particles was not uniform for CD-SiO_2 1:0.1 nanocomposite. Nearly spherical silica particles of size less than 100 nm were observed in the SEM images, and carbon dots with a size <5 nm were homogeneously distributed throughout the outer surface of the silica spheres. On the other hand, spherical silica particles of size ~200–250 nm were observed in the SEM images of the CD-SiO_2 1:0.25 nanocomposite, and the carbon dots with size <5 nm were homogeneously distributed throughout the outer surface of the silica spheres which shows that CDs were successfully embedded in the SiO_2 structure. The results of the TEM analysis performed on the CD-SiO_2 1:0.25 nanocomposite (Fig. 9) were consistent with that of the SEM results as it showed successful embedding of carbon dots over silica spheres.

FTIR spectra of the carbon dot-embedded silica nanocomposites were recorded further and are presented in Fig. 10 in which a broad band around 3300 cm^{-1} was visible that corresponds to O–H stretching vibrations of the hydroxyl groups. A small peak at 2972 cm^{-1} could be ascribed to C–H methyl group asymmetrical stretching.[44] The characteristic peak at 1636 cm^{-1} corresponds to that of the graphite core of C-dots.[45] The stretching bands of C–O (alkoxy) are observed at 1044 cm^{-1}. The signals at 1085 cm^{-1} obtained for the CD-SiO_2 nanocomposites correspond to the Si–O(Si) asymmetric stretching bands whereas the smaller peaks at around 880 cm^{-1} are related to the Si–O–C bonding which is an evidence for the interaction between silica and carbon dots in the nanocomposite.[46] The small peak around 1574 cm^{-1} is assigned to the bending mode of C–N–H.

Table 1 The average lifetime and the three different lifetime components of the carbon dots and carbon dot embedded silica nanocomposites

Sample code	τ_1 (s)	τ_2 (s)	τ_3 (s)	Life time (ns)
Pure carbon dots	4.28×10^{-9}	9.12×10^{-10}	1.18×10^{-8}	4.77
CD-SiO_2-1:0.05	4.76×10^{-9}	1.33×10^{-9}	1.02×10^{-8}	6.71
CD-SiO_2-1:0.1	1.30×10^{-9}	7.14×10^{-9}	1.29×10^{-8}	8.49
CD-SiO_2-1:0.25	3.96×10^{-9}	8.67×10^{-10}	1.04×10^{-8}	6.34

Application study of the CD-SiO_2 nanocomposite

To evaluate the practical application of the synthesized CD-SiO_2 nanocomposite as a hydrological tracer for groundwater studies, laboratory-scale continuous flow column experiments have been conducted. The movement of the nanotracer through fine sand and soil columns has been studied. Results of the column experiments conducted with fine sand wherein

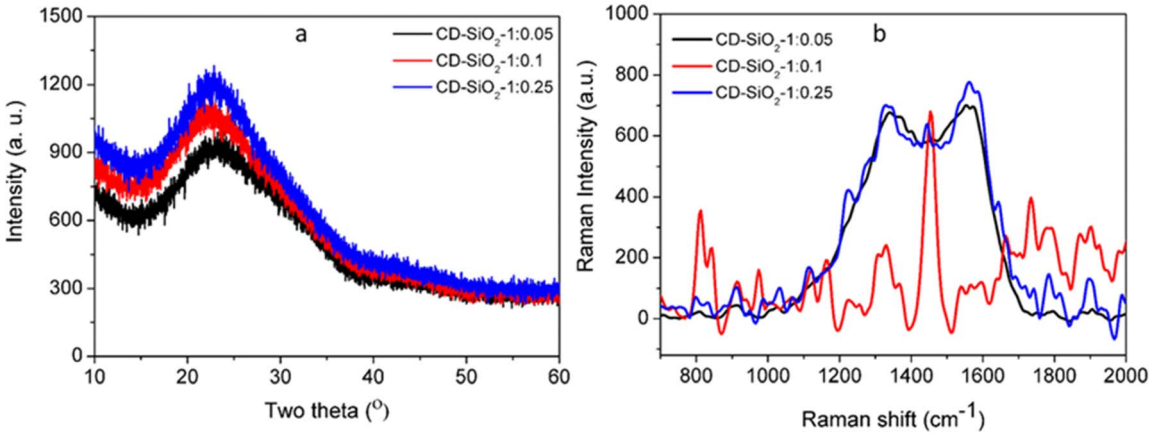

Fig. 7 (a) X-ray diffractograms and (b) Raman spectra of the carbon dot embedded silica nanocomposite.

different concentrations of the tracers were injected at the top of the sand column are provided in Fig. 11.

Fig. 11a represents the breakthrough curve when 100 mg of the nanotracer was injected into the sand column wherein the deionized water was continuously passed at a constant flow rate of 5 mL min^{-1} and the tracer movement was monitored by measuring the UV-visible absorbance of the samples collected at definite intervals after tracer injection. The movement of the developed tracer was faster through the sand column and a major concentration of the injected tracer was collected from the outlet in 8 minutes for the CD and CD-SiO_2 nanocomposite. The amount of the tracer regained was calculated to be ~97% and ~98% respectively for the CD and CD-SiO_2 nanocomposite.

Methylene blue dye (100 mg) was also used as a tracer in the study which shows that the movement of the dye tracer through the column was much slower with a recovery rate of only 7.29% in 90 minutes thus revealing the efficiency of the nanotracer developed. A clear difference in the breakthrough curve obtained for the nanotracer and the dye tracer (MB) is attributed to the different diffusion rates for the two types of tracers.[47] Moreover, the interaction of the dye molecules with solid surfaces is complex due to the pH-dependent protonation and deprotonation thereby changing the net charge of the

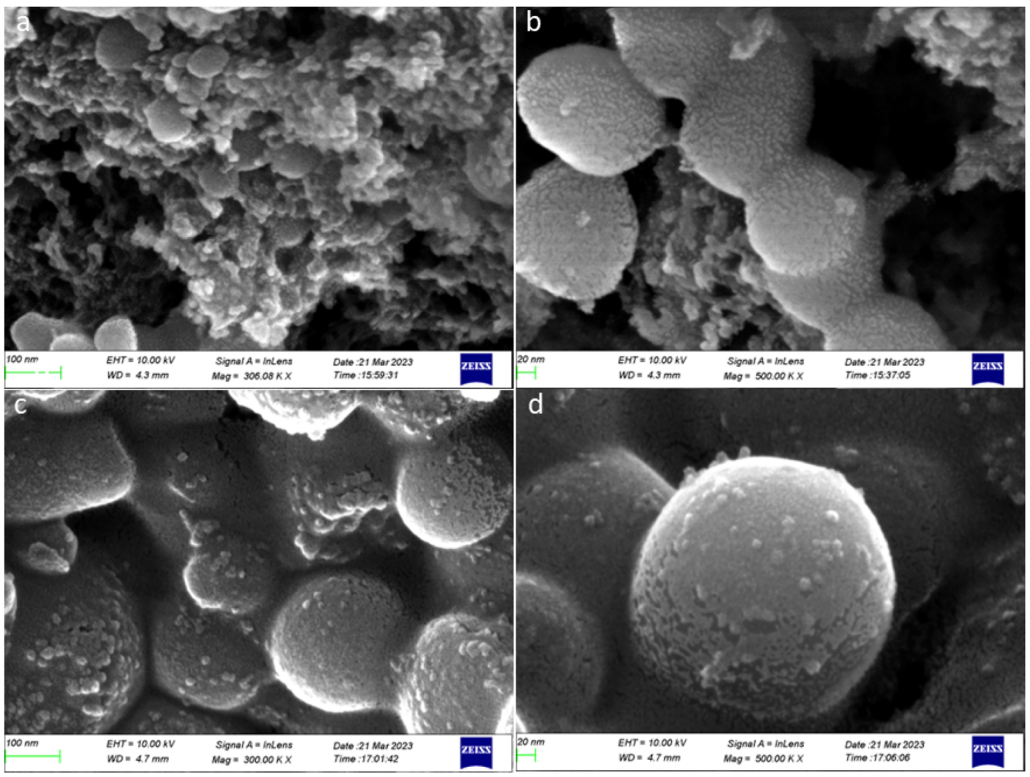

Fig. 8 FE-SEM analysis of (a and b) CD-SiO_2 1:0.1 nanocomposite and (c and d) CD-SiO_2 1:0.25 nanocomposite.

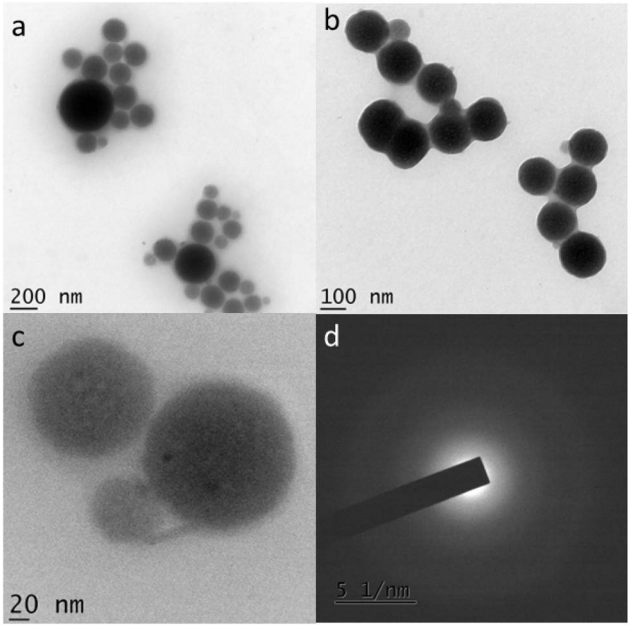

Fig. 9 TEM analysis of the CD-SiO_2 1:0.25 nanocomposite (a–c) at different magnifications and (d) SAED pattern.

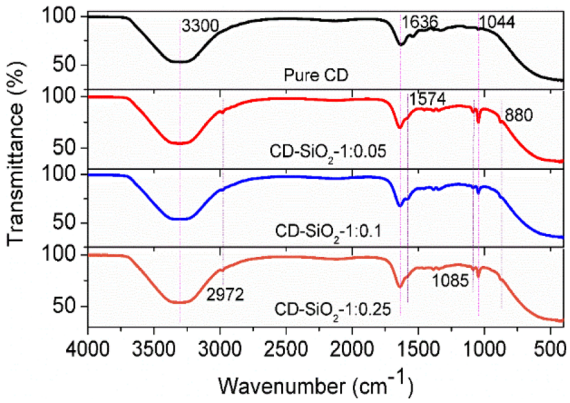

Fig. 10 FTIR spectra of pure carbon dots and carbon dot embedded silica nanocomposites.

molecule.[48] The adsorption of dye molecules onto the sand particles out of van der Waals or ion exchange interactions[49] may slow down the movement of the dye tracer through the sand column thus reducing the recovery rate. In the case of carbon dots, the surface is negatively charged as evidenced from the negative zeta potential value and their adsorption on to the sand column is relatively low under the effect of electrostatic repulsion.

When the concentration of the tracer injected into the sand column was increased from 100 mg to 200 mg, it was observed that the CD-SiO_2 nanocomposite performed better than that of pure CD in terms of faster detection and recovery of the tracer as shown in Fig. 11b. The time at which the maximum recovery of the nanotracer was obtained was 10 min and 8 min respectively for the CDs and CD-SiO_2 nanocomposites at higher concentrations of injection and the recovery percentages were ~91 and ~97% respectively. Similarly, the column experiments were conducted using soil as the filling material under similar experimental conditions and the results obtained are presented in Fig. 12.

Even though the movement of the CD-SiO_2 nanocomposite tracer was faster through the soil column with a maximum detection of around 8 minutes, the amount of the tracer regained was only ~11%. On the other hand, the time of maximum tracer detection was around 14 minutes in the case of pure CDs and the amount of tracer regained was ~33%. This lower recovery rate of CD-SiO_2 at low concentration (100 ppm) could be attributed to the stickiness tendency of the material towards the packed material (soil) used in the column.[21] But as the injected tracer concentration is increased from 100 to 200 ppm, the recovery rate of the tracer was improved from ~11% to ~28% in the case of the CD-SiO_2 nanocomposite and the time of maximum detection was improved to 8 min (from 14 min) in the case of pure CD. The effect of concentration of the tracer injection is depicted clearly in Fig. 12c which corresponds to tracer injection at relatively higher concentrations.

As the concentration of the CD nanotracer is increased to 350 mg, even though the recovery rate of the tracer is significantly improved to ~94%, the time at which maximum recovery of the tracer occurred increased to around 18 min. On the other hand, it is quite interesting to observe that as the concentration of the CD-SiO_2 nanotracer is increased to around 490 mg, about 99% of the nanotracer could be regained and the detection was very faster with the time of maximum detection being 6 minutes.

The same trend in the breakthrough curve is observed in Fig. 12 for the carbon dots as well as the carbon dot-silica nanotracer but with a delayed response by the pure CD nano tracer. On the other hand, the retrieval rate of the nanotracer was high for the pure CDs at low concentrations of 100 and 200 mg tracer injections and the retrieval rate was high for CD-SiO_2 at a high concentration of 490 mg. This can be explained by the heterogeneity as well as the electrostatic interactions by the porous soil media which affect the particle deposition and retention.[50] The few high-intensity peaks noticed for the nanotracer may be due to late arrivals of the tracer clusters indicating the stickiness tendency of the nanotracer towards the soil column.[21] The electrostatic forces associated with carbon dot and CD-SiO_2 nanotracers are different considering the particle size differences of the CDs and CD-SiO_2. The particle size of pure CDs was much lesser (<10 nm) whereas the size was ~200–250 nm for the CD-SiO_2 nanocomposite. At lower concentrations, relatively larger particles could not pass through the porous structure of the soil column very easily as it is hindered by the strong electrostatic repulsive forces whereas the smaller particles are allowed to pass through the column hence the higher retrieval rate for the carbon dot tracer. At higher concentrations, electrostatic repulsive forces of the larger sized CD-SiO_2 particles are compressed to some extent[51] which allows it to pass through the porous soil column and hence the higher retrieval rate.

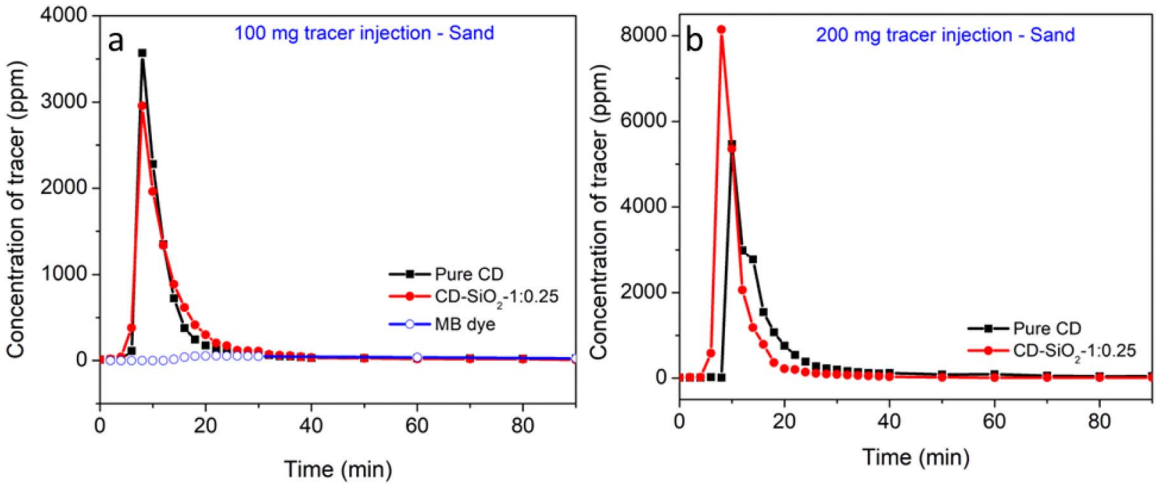

Fig. 11 Breakthrough curves in the injected tracer study with (a) 100 mg and (b) 200 mg injection, showing tracer movement through the sand column with time.

Molecular diffusion and hydrodynamic dispersions are the two important mechanisms that play their role in the spreading of a dissolved mass[52] as it moves along with water in continuous flow column studies. Molecular diffusion is predominant only at the pore scale of investigation, whereas at local scales of few meters in column experiments, hydrodynamic dispersion is usually highly significant.[53]

The diffusion coefficients were calculated further for the CD and CD-SiO_2 nanotracers using the Stokes–Einstein equation.[54]

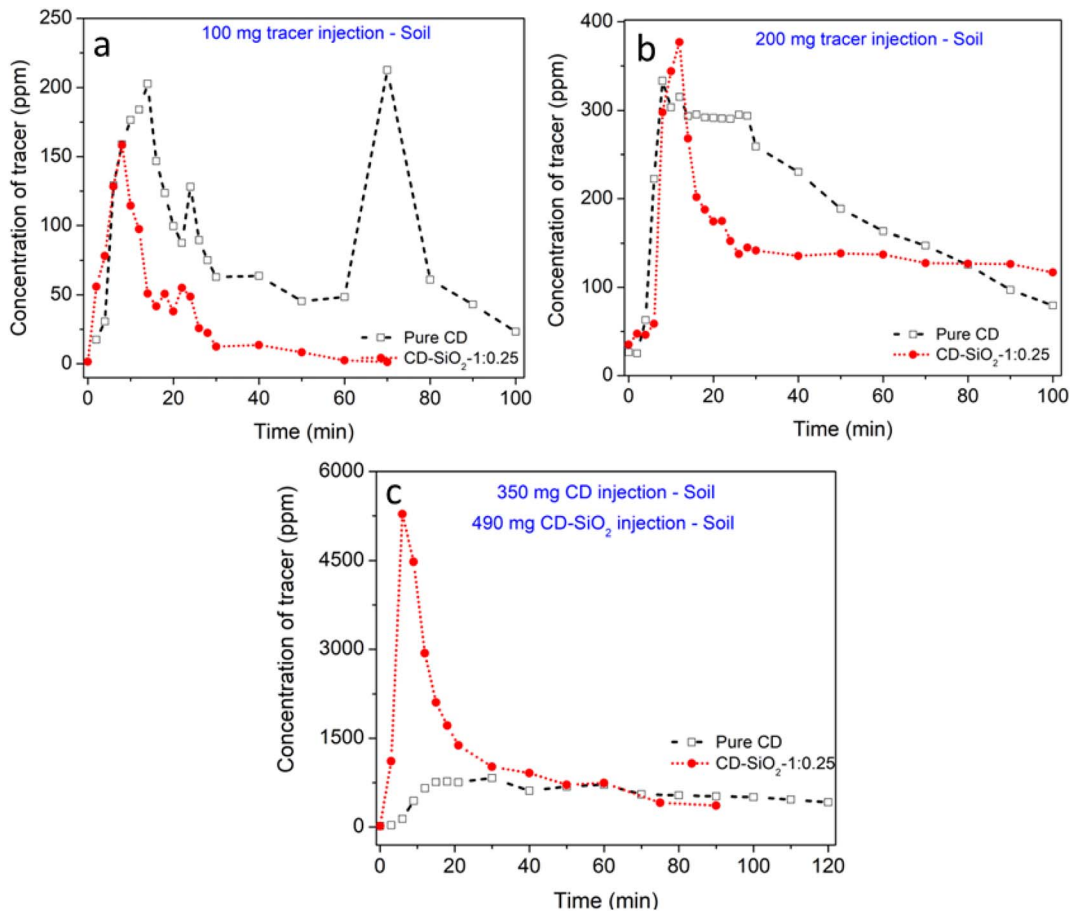

Fig. 12 Breakthrough curves in the injected tracer study with (a) 100 mg, (b) 200 mg and (c) 350, 490 mg injection, showing the tracer movement through the soil column with time.

$$D_\infty = k_B T / 3\pi\mu d_p$$

where D_∞ is the aqueous diffusion coefficient ($cm^2\ s^{-1}$), k_B is the Boltzmann constant (1.38065×10^{-23} J K^{-1}), T is the absolute temperature (293.15 K), μ is the dynamic viscosity (g $cm^{-1}\ s^{-1}$) and d_p is the diameter of the nanoparticle (cm).

The calculated diffusion coefficient values were 9.073×10^{-8} and 7.59×10^{-5} $m^2\ s^{-1}$ respectively for the CD and CD-SiO_2 nanotracers.

The results of the present study were comparable with that of the reported literature (Table 2) on nanotracers developed *via* different routes and subjected to continuous flow column experiments for studying hydrology-related applications.

Moreover, the fabrication of the nanotracer in the present study without incorporating any fluorescent dye molecules for traceability suggests the eco-friendliness of the nanocomposite system.

The results of the continuous flow column experiments carried out using injected tracers are summarized in Table 3.

Hence, it can be summarized that the developed carbon dot embedded silica nanocomposites can be very well applied as a nanotracer in hydrogeological studies as they exhibit faster detection and recovery in the laboratory scale sand/soil column experiments. The optimal size of the developed nanotracer can ensure its traceability in complex environmental scenarios while retaining the original optical properties of the nanomaterial.

Experimental

Materials

Glucose (α-D-glucose, anhydrous, 96%), ethylene diamine, and tetra ethyl ortho silicate (TEOS) were procured from Sigma-Aldrich and were used as purchased.

Methods

Synthesis of carbon dots (CDs). A microwave-assisted synthesis technique was used for the synthesis of carbon dots (CDs). In a typical experiment, 1 g of glucose was mixed with 10 mL of distilled water by ultrasonication for 10 minutes. Separately, 1 g of ethylene diamine was added to 15 mL of absolute ethanol under sonication. These two solutions were mixed by stirring them for 30 minutes using a magnetic stirrer at room temperature. The homogeneous solution was further treated under microwaves (600 W) for about 5 minutes. Color change from colorless to golden yellow was observed for an increase in the microwave exposure time indicating the extent of the formation of carbon dots.

Synthesis of silica sol. Silica sol was synthesized from the precursor, tetra ethyl ortho silicate (TEOS). Tetraethyl ortho silicate (TEOS), isopropyl alcohol (IPA), and acidified water (0.001 N HCl) were mixed in the molar ratio of 1 : 4 : 16 in a clean beaker and stirred well for about 2 hours using a magnetic stirrer when the slightly turbid solution turns to a clear silica sol. In a typical experiment, about 0.8668 g of tetra ethyl ortho silicate was mixed with about 1.0002 g of isopropyl alcohol in a beaker, and about 1.1984 g of acidic water was added followed by stirring for about 2 hours to get the silica sol.

Synthesis of the carbon dot embedded silica nanocomposite (CD-SiO_2). The carbon dot-embedded silica nanocomposite (CD-SiO_2) was synthesized *via* a co-polycondensation method. Silica sol synthesized previously was added dropwise to the solution containing carbon dots and stirred continuously for about 3 hours wherein the color of the solution changed to milky white. The milky white solution was then subjected to microwave treatment (600 W) for about 5 minutes to synthesize the carbon dot-embedded silica nanocomposites (CD-SiO_2). The formation of the CD-SiO_2 nanocomposite was indicated by a color change from milky white to dark yellow after the

Table 2 Comparison of the present work with reported ones

Reference literature	Vitorge *et al.*,[55] 2014	Berson *et al.*,[14] 2024	Spitzmüller *et al.*,[56] 2023	Sharma *et al.*,[57] 2012	Present work
Tracer used	Silver labelled silica nanoparticles	Core–shell reporting nanoparticles with dual emission	Temperature triggered core–shell silica nanoparticle tracer	DNA and iron oxide incorporated PLA spheres	Carbon dot embedded silica nanocomposite tracer
Size of the tracer (nm)	150	72	70	∼350	∼250
Column height (cm)	15	100	100	24.5	20
Column diameter (cm)	2.6	5.3	5.3	2.54	3
Porous medium	Hostun sand	Quartz sand	Coarse quartz sand	Quartz sand	Fine beach sand
Flow rate (mL min^{-1})	0.166667	243	240	6.7	5.0
Concentration of the tracer (g)	0.0194	0.5	—	0.1	0.1
$Tracer_{minimum}$ (min)	—	2.5	2.85	6	2
$Tracer_{maximum}$ (min)	—	3.7	4.41	16	8
Recovery rate (%)	18	82	78.5	—	98

Table 3 Summary of the injected tracer study conducted

Filling material	Sample	Tracer concentration (mg)	Tracer recovery (%)	Time duration of the experiment (min)	Time of maximum recovery (min)
Sand	CD	100	97.04	90	8
Sand	CD-SiO_2 1:0.25	100	98.29	90	8
Sand	CD	200	90.53	90	10
Sand	CD-SiO_2-1:0.25	200	96.79	90	8
Sand	Methylene blue dye	100	7.29	100	22
Soil	CD	100	33.22	100	14
Soil	CD-SiO_2-1:0.25	100	10.56	70	8
Soil	CD	200	38.77	100	8
Soil	CD-SiO_2-1:0.25	200	27.69	90	12
Soil	CD	350	93.97	120	18
Soil	CD-SiO_2-1:0.25	490	98.91	90	6

microwave treatment. Carbon dots and silica were mixed in different weight ratios of 1 : 0.01, 1 : 0.05, and 1 : 0.25 to prepare the CD-SiO_2 nanocomposites of different compositions herein labeled as CD-SiO_2-0.01, CD-SiO_2-0.05 and CD-SiO_2-0.25 respectively.

Characterization

The synthesized carbon dots (CD) and carbon dot embedded silica nanocomposites (CD-SiO_2) are characterized using UV-visible spectra analysis, X-ray diffraction (XRD) analysis, Fourier Transform Infrared (FTIR) analysis, Field Emission Scanning Electron Microscopic (FESEM) analysis, Transmission Electron Microscopic analysis (TEM), photoluminescence spectroscopy (PL), Raman spectroscopy, and lifetime analysis. X-ray diffraction analysis of the powder samples was carried out using a PANALYTICAL, Aeris Research XRD instrument in the 2θ range 10°–80° using Cu Kα radiation ($\lambda = 1.54$ Å). The infrared spectrum of the nanocomposite was recorded in a PerkinElmer Spectrum Two FTIR spectrometer, in the range 4000–400 cm^{-1}, using a Universal ATR accessory (UATR Two). UV-visible spectra of the carbon dots and the nanocomposites were collected using a UV-visible spectrophotometer (Model: Evolution, Thermo Fischer) in the wavelength range of 200–800 nm. The morphology of the samples was observed using a Hitachi SU6600 Variable Pressure Field Emission Scanning Electron Microscope (FESEM) operated at 5 kV. High-resolution transmission electron microscopic analysis of the samples was performed in an HRTEM: Jeol/JEM 2100 model instrument (200 kV, LaB6 electron gun, point resolution 0.23 nm and lattice resolution 0.14 nm). Photoluminescence spectra collection and lifetime analysis of the samples were conducted using a Horiba fluorolog fluorescence spectrometer coupled with an integrating sphere and lifetime detector. Raman analysis was carried out using a WITec alpha300 ra – confocal Raman microscope.

Application study of CDs and CD-SiO_2 nanocomposite

The application of the synthesized carbon dots (CDs) and carbon dot-embedded silica (CD-SiO_2) nanocomposite as a tracer for groundwater studies was tested *via* injected tracer studies under laboratory conditions. Continuous flow column experiments were conducted to ascertain the application of the synthesized material as an injected tracer. Glass columns of length 30 cm and diameter 3 cm were used for the study in which sand and soil were used as the filling materials. The fine sand and soil samples subjected to the experiments were collected from geologically different sites during the project period and were further processed and characterized for their physicochemical properties (Table S2†) before conducting the experiments. The filling material (sand/soil) was filled in the column to a constant height of about 20 cm and distilled water was allowed to flow through the filled column at a constant flow rate of 5 mL per minute using a peristaltic pump. Distilled water was continuously passed through the filled column for about 3 hours to reduce any background contamination from the filling materials. The synthesized CDs and CD-SiO_2 were injected into the top of the filled column at different concentrations of 100 mg and 200 mg and the movement of the nanotracer was monitored further by collecting the water samples from the outlet of the column at 2 min intervals up to 30 minutes and at 10 min intervals up to about 1.5 hours. The amount of carbon dots present in the collected water sample was tested using a UV-visible spectrophotometer.

Quantification of the carbon dots present in the water sample was based on the fitting of the spectrophotometric data obtained to a calibration curve previously constructed. A series of carbon dot standard solutions of different concentrations (100–500 ppm) were used to construct the calibration curve for CDs in the UV-visible spectrophotometer. The amount of the nanotracer that can be regained after injecting through the filled column was calculated further to understand the applicability of the synthesized material as a tracer for groundwater studies.

$$\text{Amount of the nano tracer regained (\%)} = \frac{\sum \text{amount of CD collected at definite intervals (mg)}}{\text{amount of CD injected to the column (mg)}} \times 100$$

Conclusions

A carbon dot embedded silica nanocomposite was successfully synthesized in the present work using a microwave-assisted co-

polycondensation method. The UV-visible absorbance spectra and FTIR spectra recorded for the nanocomposite clearly show the interaction between the carbon dots and silica particles. Intense green emission was shown by the synthesized nanocomposite when excited at a wavelength of 320 nm and the photoluminescence intensity was found to be dependent on the concentration of carbon dots in the nanocomposite. The average lifetime of the CD-SiO_2 nanocomposites was higher than that of pure carbon dots and the presence of embedded carbon dots in the nanocomposite samples was apparent in the Raman spectra showing the presence of both amorphous and crystalline carbon phases in the core structure. Spherical silica particles of size ~200–250 nm were observed in the SEM images and the carbon dots with size <5 nm were homogeneously distributed throughout the outer surface of the silica spheres which shows that CDs were successfully embedded in the SiO_2 structure. The applicability of the synthesized CD-SiO_2 nanocomposite as a hydrological tracer for groundwater studies was confirmed by conducting laboratory-scale continuous flow column experiments by varying the filling materials and concentration of the injected tracer at a constant flow rate. From the results obtained for the laboratory scale sand/soil column experiments it can be concluded that the developed carbon dot embedded silica nanocomposite can be very well applied as a nanotracer in hydrogeological studies as it exhibits faster detection and recovery.

Thus, it is envisaged that the nanotracer developed in the present work may contribute towards managing the challenges involved in groundwater flow analysis owing to its better traceability. The nanotracer will be useful for subsurface investigations as well as for the characterization and management of contaminant sites and hence particularly relevant to hydrogeological applications. The nanocomposite tracer can also offer a sustainable solution for the characterization of solute transport in complex environmental scenarios and hence will be able to address future climatic and anthropogenic perturbations.

Data availability

The data in the manuscript will be made available upon requesting the corresponding author.

Author contributions

The concept of this study was developed by SVS. The experimental work was carried out by AP with guidance from SVS. JKK and RTR were involved in the critical revision of the article. All the authors read and approved the final manuscript.

Conflicts of interest

There are no conflicts to declare.

Acknowledgements

The authors acknowledge the Executive Director, CWRDM, and the Head-Ecology and Environment Research Group, CWRDM, for providing the necessary facilities to carry out the research work. Ms Anju Balakrishnan and Ms Dayalakshmi CB are acknowledged for carrying out part of the work as MSc Dissertation. DST and the SAIF, Kottayam are acknowledged for PL, lifetime, and Raman analysis. All the members of the Ecology and Environment Research Group, CWRDM, are acknowledged for providing general assistance. Acknowledgment is due to the Kerala State Government for providing the plan fund to carry out the work.

Notes and references

1 A. Boretti and L. Rosa, *npj Clean Water*, 2019, **2**, 15.
2 R. K. Mishra, S. S. Mentha, Y. Misra and N. Dwivedi, *Water-Energy Nexus*, 2023, **6**, 74–95.
3 G. V. Evans, *Appl. Radiat. Isot.*, 1983, **34**, 451–475.
4 V. Cao, M. Schaffer, R. Taherdangkoo and T. Licha, *Water*, 2020, **12**, 653.
5 A. Cozma, C. Baciu, M. Moldovan and I. Pop, *Procedia Environ. Sci.*, 2016, **32**, 211–220.
6 B. W. Abbott, V. Baranov, C. Mendoza-Lera, M. Nikolakopoulou, A. Harjung, T. Kolbe, M. N. Balasubramanian, T. N. Vaessen, F. Ciocca, A. Campeau, M. B. Wallin, P. Romeijn, M. Antonelli, J. Gonçalves, T. Datry, A. M. Laverman, J.-R. de Dreuzy, D. M. Hannah, S. Krause, C. Oldham and G. Pinay, *Earth-Sci. Rev.*, 2016, **160**, 19–42.
7 C. Leibundgut and J. Seibert, Tracer Hydrology, in *Treatise on Water Science*, ed. P. Wilderer, Oxford: Academic Press, 2011, vol. 2, pp. 215–236.
8 Y. Yurtsever and L. A. Araguas, *Environmental Isotope Applications in Hydrology: an Overview of the IAEA's Activities, Experiences, and Prospects*, International Association of Hydrological Sciences, United Kingdom, 1993.
9 P. Wachniew, *Acque Sotter.–Ital. J.*, 2015, **4**, 19–25.
10 I. Rushdi, K. F. Al-Mutlaq, A. H. El-Mubarak, M. A. Al-Saleh, M. T. El-Otaibi, S. M. M. Ibrahim and B. R. T. Simoneit, *Environ. Pollut.*, 2016, **208**, 696–703.
11 R. Benischke, *Hydrogeol. J.*, 2021, **29**, 67–88.
12 H. Haba, S. Motomura, S. Kamino and S. Enomoto, in *Handbook of Nuclear Chemistry*, ed. A. Vértes, S. Nagy, Z. Klencsár, R. G. Lovas and F. Rösch, Springer US, Boston, MA, 2011, pp. 1761–1792.
13 N. Čebašek, R. Haugsrud, Z. Li and T. Norby, *J. Am. Ceram. Soc.*, 2013, **96**, 598–605.
14 J. Berson, B. Rudolph, L. Spitzmüller, T. Kohl and T. Schimmel, *J. Hydrol.*, 2024, **637**, 131429.
15 J. Zhuang, J. Qi and Y. Jin, *Environ. Sci. Technol.*, 2005, **39**, 7853–7859.
16 S. K. Subramanian, Y. Li and L. M. Cathles, *Water Resour. Res.*, 2013, **49**, 29–42.
17 M. Abdullah Issa, Z. Z. Abidin, S. Sobri, S. Rashid, M. Adzir Mahdi, N. Azowa Ibrahim and M. Y. Pudza, *Nanomaterials*, 2019, **9**, 1500.
18 M. Y. Pudza, Z. Z. Abidin, S. Abdul-Rashid, F. M. Yassin, A. S. M. Noor and M. Abdullah, *ChemistrySelect*, 2019, **4**, 4140–4146.
19 M. Kurian and A. Paul, *Carbon Trends*, 2021, **3**, 100032.

20 Z. Hu, H. Gao, S. B. Ramisetti, J. Zhao, E. Nourafkan, P. W. J. Glover and D. Wen, *Sci. Total Environ.*, 2019, **669**, 579–589.
21 T. Warsi, L. Bhattacharjee, S. Thangamani, S. K. Jat, K. Mohanta, R. R. Bhattacharjee, R. Ramaswamy, C. Manikyamba and T. V. Rao, *Diamond Relat. Mater.*, 2020, **103**, 107701.
22 B. Sun, F. Ma, H. Zhang, N. Peng and P. Zhang, *Heritage Sci.*, 2023, **11**, 211.
23 K. Sato, R. Katakami, Y. Iso and T. Isobe, *ACS Appl. Nano Mater.*, 2022, **5**, 7664–7669.
24 Q. Zhang, R. Wang, B. Feng, X. Zhong and K. Ostrikov, *Nat. Commun.*, 2021, **12**, 6856.
25 C. M. Carbonaro, R. Corpino, M. Salis, F. Mocci, S. V. Thakkar, C. Olla and P. C. Ricci, *C*, 2019, vol. 5.
26 K. M. Omer, K. H. Hama Aziz, Y. M. Salih, D. I. Tofiq and A. Q. Hassan, *New J. Chem.*, 2019, **43**, 689–695.
27 A. Bhattacharya, S. Chatterjee, R. Prajapati and T. K. Mukherjee, *Phys. Chem. Chem. Phys.*, 2015, **17**, 12833–12840.
28 T. Balakrishnan, W. L. Ang, E. Mahmoudi, A. W. Mohammad and N. S. Sambudi, *Carbon Resour. Convers.*, 2022, **5**, 150–166.
29 H. Shabbir, T. Tokarski, D. Ungor and M. Wojnicki, *Materials*, 2021, **14**, 7604.
30 B. Wang and S. Lu, *Matter*, 2022, **5**, 110–149.
31 V. Strauss, J. T. Margraf, C. Dolle, B. Butz, T. J. Nacken, J. Walter, W. Bauer, W. Peukert, E. Spiecker, T. Clark and D. M. Guldi, *J. Am. Chem. Soc.*, 2014, **136**, 17308–17316.
32 K. J. Mintz, Y. Zhou and R. M. Leblanc, *Nanoscale*, 2019, **11**, 4634–4652.
33 M. Bayati, J. Dai, A. Zambrana, C. Rees and M. Fidalgo de Cortalezzi, *J. Environ. Sci.*, 2018, **65**, 223–235.
34 R. L. Vander Wal, A. J. Tomasek, K. Street, D. R. Hull and W. K. Thompson, *Appl. Spectrosc.*, 2004, **58**, 230–237.
35 V. Georgakilas, J. A. Perman, J. Tucek and R. Zboril, *Chem. Rev.*, 2015, **115**, 4744–4822.
36 N. K. Khairol Anuar, H. L. Tan, Y. P. Lim, M. S. So'aib and N. F. Abu Bakar, *Front. Energy Res.*, 2021, **9**, 626549.
37 P. Andrade, G. Nakazato and N. Duran, *J. Phys.: Conf. Ser.*, 2017, **838**, 012028.
38 A. Bokare, D. Nordlund, C. Melendrez, R. Robinson, O. Keles, A. Wolcott and F. Erogbogbo, *Diamond Relat. Mater.*, 2020, **110**, 108101.
39 H. Ding, X.-H. Li, X.-B. Chen, J. Wei, X.-B. Li and H.-M. Xiong, *J. Appl. Phys.*, 2020, **127**, 231101.
40 J. Chen, W. Liu, L.-H. Mao, Y.-J. Yin, C.-F. Wang and S. Chen, *J. Mater. Sci.*, 2014, **49**, 7391–7398.
41 Y. Borodko, J. Ager, G. Martí, H. Song, K. Niesz and G. Somorjai, *J. Phys. Chem. B*, 2005, **109**, 17386–17390.
42 D.-T. Tran and N. Nguyen, *Mater. Res. Express*, 2020, **7**, 045504.
43 M. L. Simeral, A. Zhang, S. M. E. Demers, H. J. Hughes, M. Abdul-Moqueet, K. M. Mayer and J. H. Hafner, *J. Phys. Chem. B*, 2021, **125**, 2031–2041.
44 S. Venu Sreekala, V. Vijayan, P. M. Abdul Azeez, B. N. Nair and U. N. S. Hareesh, *ACS Appl. Nano Mater.*, 2020, **3**, 10040–10048.
45 A. Shaikh, M. Tamboli, R. Patil, A. Bhan, J. Ambekar and B. Kale, *J. Nanosci. Nanotechnol.*, 2019, **19**, 2339–2345.
46 S. Jung Sang and T. Oh, in *IEEE Nanotechnology Materials and Devices Conference*, 2006, vol. 1, pp. 462–463.
47 A. Kittilä, M. R. Jalali, K. F. Evans, M. Willmann, M. O. Saar and X. Z. Kong, *Water Resour. Res.*, 2019, **55**, 6577–6595.
48 F. Wei, Y. Zhu, T. He, S. Zhu, T. Wang, C. Yao, C. Yu, P. Huang, Y. Li, Q. Zhao and W. Song, *ACS Omega*, 2022, **7**, 46288–46302.
49 M. A. Rauf, S. B. Bukallah, F. A. Hamour and A. S. Nasir, *Chem. Eng. J.*, 2008, **137**, 238–243.
50 C. Shen, Y. Jin, J. Zhuang, L. Tiantian and B. Xing, *Crit. Rev. Environ. Sci. Technol.*, 2019, **50**, 1–86.
51 S. Karmakar, *Recent Trends in Materials: Physics and Chemistry*, 2019, pp. 117–159.
52 M. Dentz, J. J. Hidalgo and D. Lester, *Transp. Porous Media*, 2023, **146**, 5–53.
53 V. Nguyen and D. V. Papavassiliou, *Fluids*, 2020, **5**, 79.
54 J. Zmpitas and J. Gross, *Ind. Eng. Chem. Res.*, 2021, **60**, 4453–4459.
55 E. Vitorge, S. Szenknect, J. M. F. Martins, V. Barthès and J.-P. Gaudet, *Environ. Pollut.*, 2014, **184**, 613–619.
56 L. Spitzmüller, F. Nitschke, J. Berson, A. Maercks, B. Rudolph, T. Schimmel and T. Kohl, in *Proceedings, 48th Workshop on Geothermal Reservoir Engineering*, Stanford, CA, USA, 2023.
57 A. N. Sharma, D. Luo and M. T. Walter, *Environ. Sci. Technol.*, 2012, **46**, 8928–8936.